# Imaging of *s* and *d* Partial-Wave Interference in Quantum Scattering of Identical Bosonic Atoms

Nicholas R. Thomas,[1] Niels Kjærgaard,[1,*] Paul S. Julienne,[2] and Andrew C. Wilson[1]
[1]*Department of Physics, University of Otago, Dunedin, New Zealand*
[2]*National Institute of Standards and Technology, 100 Bureau Drive, Stop 8423, Gaithersburg, Maryland, 20899-8423 USA*
(Received 19 May 2004; published 22 October 2004)

We report on the direct imaging of *s* and *d* partial-wave interference in cold collisions of atoms. Two ultracold clouds of $^{87}$Rb atoms were accelerated by magnetic fields to collide at energies near a *d*-wave shape resonance. The resulting halos of scattered particles were imaged using laser absorption. By scanning across the resonance we observed a marked evolution of the scattering patterns due to the energy dependent phase shifts for the interfering *s* and *d* waves. Since only two partial-wave states are involved in the collision process the scattering yield and angular distributions have a simple interpretation in terms of a theoretical model.

DOI: 10.1103/PhysRevLett.93.173201 PACS numbers: 34.50.–s, 03.65.Nk, 32.80.Pj, 39.25.+k

Atomic collisions are a classic topic of quantum mechanics [1,2]. With the advent of laser cooling [3], confining and cooling various atomic species to submillikelvin temperatures became possible and gave rise to a wealth of experiments in which quantum effects in collisions at very low energies—cold collisions—were observed [4]. Knowledge about cold collisions paved the way for exciting new developments in experimental atomic physics. Collisions played a crucial role in the achievement of Bose-Einstein condensation [5] and Fermi degeneracy [6] in dilute atomic vapors by mediating thermalization during evaporative cooling and accounting for stability [7]. For atoms at temperatures associated with the quantum degenerate regime the essential interaction properties are determined by a single atomic parameter, the scattering length, because all elastic scattering has an isotropic (*s*-wave) nature at such low energies. The scattering length may exhibit a pronounced dependency on external magnetic fields giving rise to so-called Feshbach resonances [8] which have recently been exploited to create ultracold molecules [9] and molecular Bose-Einstein condensates (BECs) [10].

To date, most experiments on cold collisions of atoms have been carried out using magneto-optical traps (MOTs) or magnetic traps which suffer from the disadvantages that no collision axis is singled out or the collision energy cannot be varied over a wide range [4,11]. If no fixed collision axis is present, anisotropic scattering, as occurs for collision energies above the *s*-wave regime, will be obscured by spatial averaging. One solution to this problem was provided in the ''juggling'' MOT experiment [12], where a cloud of cesium atoms was laser cooled to 3 $\mu$K and ejected vertically from a trap to collide with a previously launched cloud at energies up to 160 $\mu$K. Scattered atoms were detected using a spectroscopic technique revealing interference between *s* and *p* partial waves. In experiments on BECs, a collision axis was also selected using Bragg scattering to accelerate part of the atomic cloud, and pure *s*-wave scattering halos were directly imaged [13].

In this Letter, we report experiments on the collision of two bosonic atomic clouds, initially confined in a magnetic double-well potential and evaporatively cooled to a temperature just above the phase transition for Bose-Einstein condensation. Collisions at a selectable energy occur when the trapping potential is continuously modified to a single-well configuration. The atomic clouds accelerate from the sides of the harmonic potential and collide at the center of the well. The resulting scattering is equivalent to cold collisions of counterpropagating ultracold pulsed atomic beams. Angular resolved detection of scattered atoms is obtained using laser absorption imaging. Specifically, we consider atomic clouds of doubly spin-polarized $^{87}$Rb which are cooled to a temperature of $\sim$225 nK and accelerated to collide with energies in the range from 87 to 553 $\mu$K as measured in units of Boltzmann's constant $k_B$. In this energy interval a *d*-wave shape resonance is known to occur [14]. We observe scattering patterns evolving from *s*-wave-like to *d*-wave-like distributions via intermediate $s + d$ interfering scattering states which expose the quantum mechanical origin of the process.

Quantum scattering of two particles under our conditions is conveniently described in the partial-wave formalism. The wave function for the relative motion is written $\psi = e^{ikz} + f(\theta)e^{ikr}/r$, where $k$ is the magnitude of the relative wave vector of the colliding particles. The first term of this sum represents an incoming plane wave traveling along the $z$ axis, while the second term represents a radially outgoing scattered wave with an amplitude which depends on the angle $\theta$ to the $z$ axis, (see, e.g., [15]). Using a partial-wave expansion of $\psi$, the scattering amplitude for identical bosons is expressed as $f(\theta) = \sum_{l\,\mathrm{even}}(2l + 1)(e^{2i\eta_l} - 1)P_l(\cos\theta)/ik$, where $P_l$ is the

  

Legendre polynomial of order $l$ and $\eta_l$ are the partial-wave phase shifts. The $l$th term in the expansion represents particles having orbital angular momentum $l\hbar$ and the sum only runs over even $l$, since odd partial waves are forbidden by the requirement of a totally symmetric wave function for identical bosonic particles. In the present case, where only $l = \{0, 2\}$ terms ($s$ and $d$ waves) contribute [16], the scattering amplitude is

$$f(\theta) = [\underbrace{(e^{2i\eta_0} - 1)}_{s} + \underbrace{5(e^{2i\eta_2} - 1)(3\cos^2\theta - 1)/2}_{d}]/ik, \tag{1}$$

and the differential cross section $d\sigma/d\Omega = |f(\theta)|^2$ has an angular pattern which depends crucially on the quantum mechanical interference between the partial-wave states as dictated by the phase shifts. Assuming the collisions to occur in free space, scattered particles observed in the center of mass frame will be distributed over a ballistically expanding sphere (the so-called Newton sphere) according to the differential cross section. If the scattered particles are detected using absorption imaging, the distribution on this sphere will be projected onto a plane by the Abel transformation [17]. Figure 1 illustrates this in the case of pure $d$-wave scattering and imaging along a direction perpendicular to the collision axis.

In our experiment, $^{87}$Rb atoms collected in a MOT were optically pumped into the $|F = 2, m_F = 2\rangle$ hyperfine substate and loaded into a Ioffe-Pritchard magnetic trap in the quadrupole-Ioffe configuration [18]. The trapping potential is cylindrically symmetric and harmonic, characterized by radial and axial oscillation frequencies of $\omega_r/2\pi = 275$ and $\omega_z/2\pi = 16$ Hz, respectively. After rf evaporative cooling to a temperature of 12 $\mu$K, the trap was adiabatically transformed to a double-well configuration [19], splitting the atomic cloud in half along its long dimension ($z$) by raising a potential barrier. The $z$ axis is horizontal so that the influence from gravity is unimportant. An additional rotating bias field of 0.5 mT is applied just before forming the double well to avoid Majorana spin-flip atom loss at the two trap minima, where the magnetic field would otherwise become zero. When fully separated the two clouds were 4.3 mm apart and the trap frequencies were $\omega_r/2\pi = 60$ Hz and $\omega_z/2\pi = 14$ Hz near the well minima. Further evaporative cooling lowered the temperature to 225 nK in each well (as compared to the BEC transition temperature of 100 nK), and the total number of remaining atoms was $4 \times 10^5$. There is a slight difference between the properties of the two clouds due to a small residual tilt in the potential. Subsequently the separation of the clouds was adiabatically adjusted to select the potential energy gained when the trap is rapidly converted back to a single well. To increase the cloud densities the rotating bias field was reduced to 0.2 mT. The collision is initiated by rapidly ramping from a double- to a single-well configuration, accelerating the clouds towards the potential minimum positioned between them. The trapping configuration for the collision has frequencies $\omega_r/2\pi = 155$ Hz and $\omega_z/2\pi = 12$ Hz and remains unchanged until the end of the experiment. After the collision we waited for one-quarter of the radial trap period, so that atoms were at maximum radial extension, before acquiring an absorption image using a 40 $\mu$s pulse of resonant light and a charge coupled device camera. The 3D distribution of scattered atoms is projected onto a plane giving the column density distribution. We obtained the collision energy and the corresponding uncertainty from a fit to cloud positions measured before and after the collision. The collision energy, expressed in temperature units, is $T = \mu v^2/2k_B$, where $\mu$ is the reduced mass of the particles and $v$ is the relative velocity of the two clouds.

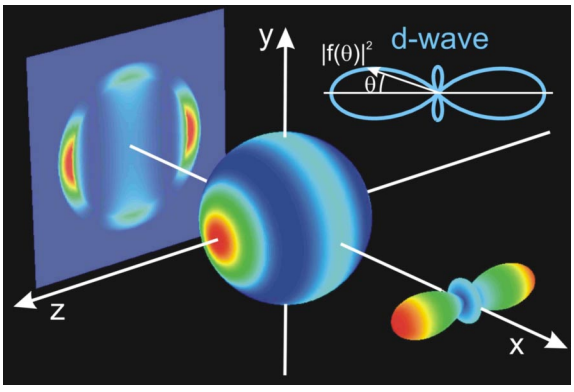


FIG. 1 (color online). Illustration of the process of using absorption imaging for the detection of scattered particles. We present the case of pure $d$-wave scattering occurring at the origin for particles coming in along the $z$ axis. Scattered particles will be situated on an expanding sphere and distributed according to the $d$-wave angular emission pattern $|f(\theta)|^2$. Absorption imaging along the $x$ axis projects this distribution onto the $yz$ plane.

Figure 2 shows absorption images of scattering acquired at collision energies in the range from 87 to 348 $\mu$K. Scattering halos of particles with an elliptical envelope are clearly visible as are the outgoing clouds of unscattered atoms. The major and minor semiaxes of the former, and the distance between the latter, increase linearly with $\sqrt{T}$ due to the fixed time of acquisition after collision. The total number of scattered particles $N_{sc}$ was determined by integrating the column density over the image frame and using a suitable interpolation to bridge the areas hidden by the outgoing clouds of unscattered atoms.

The observed scattering yield is interpreted in terms of a coupled-channels theoretical model that includes the ground state singlet and triplet potentials and all spin-dependent interactions. The triplet potential has a van der Waals $C_6$ constant of 4707 a.u. (1 a.u. $= 9.5734 \times 10^{-26}$ J nm$^6$) and a scattering length of 98.96 a.u. (1 a.u. $= 0.052\,918$ nm) [20]. Figure 3(a) presents the

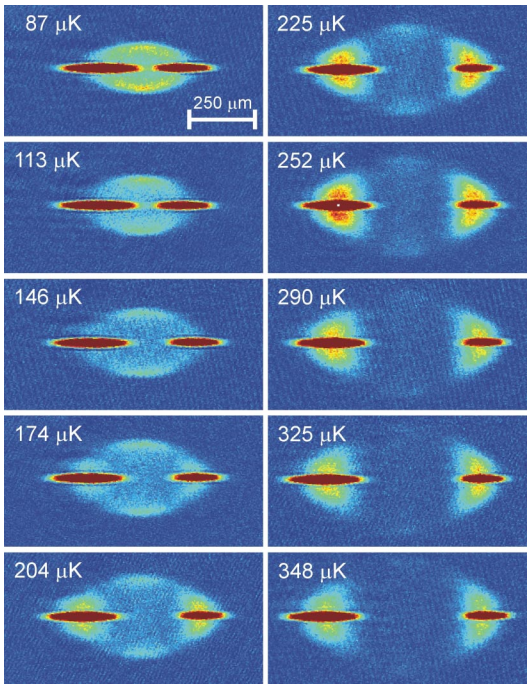


FIG. 2 (color online). Absorption images acquired at a quarter of a radial trap period after the collision of two doubly spin-polarized Rb clouds (visible as dark ellipses) for various collision energies. The halos of scattered particles have elliptical envelopes since they are evolving in an anisotropic harmonic trap which is weakest in the horizontal direction ($z$ direction). At the selected time of acquisition the scattering halos have the maximum radial excursion in the trap.

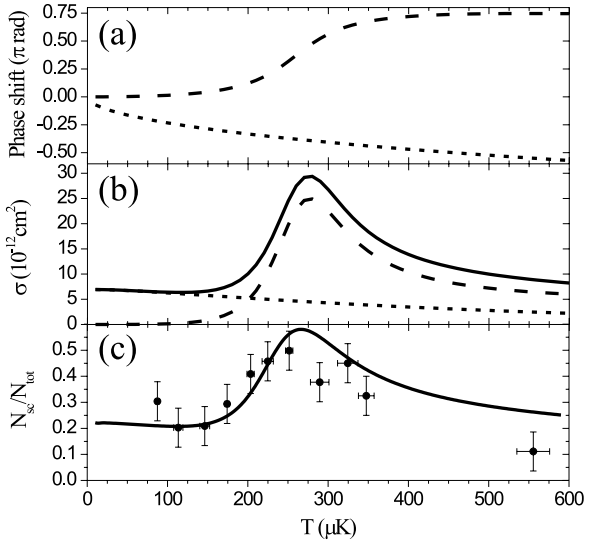


FIG. 3. Dependence on collision energy. (a) The $s$ (dotted line) and $d$ (dashed line) partial-wave phase shifts from the theoretical model. (b) The $s$-wave (dotted line), $d$-wave (dashed line), and total (solid line) cross sections calculated from the model partial-wave phase shifts. (c) The measured scattered fraction of atoms $N_{sc}/N_{tot}$ (filled circles). The black curve shows the fraction as given by the model cross section when depletion of the colliding atom clouds is accounted for.

partial-wave phase shifts for the $l = 0$ and 2 channels with total projection quantum number $m_F = 4$ when two $|F = 2, m_F = 2\rangle$ atoms collide in a total magnetic field of 0.22 mT, the bias field of this experiment (there is negligible difference at zero field). Using Eq. (1) these phase shifts give the $s$-wave, $d$-wave, and total cross sections shown in Fig. 3(b). In Fig. 3(c) we present the fraction of scattered atoms $N_{sc}/N_{tot}$ versus the collision energy as measured in our experiments. Since $N_{sc}/N_{tot}$ is on the order of 40% close to the resonance (i.e., large depletion), the number of scattered particles is not proportional to the total elastic cross section $\sigma(T)$. As a result, the observed $d$-wave resonance peak is not very pronounced even though the total cross section grows by a factor of $\sim$4 with respect to the zero energy limit. However, when the effect of depletion is included [21] we obtain good agreement between the experimental and theoretical scattering fractions [Fig. 3(c)]. The model predicts the $d$-wave resonance to occur at 275 $\mu$K, and the measurements are consistent with this to within 25 $\mu$K.

As is obvious from Fig. 2, the scattered particles are emitted in spatial patterns which depend on the collision energy. It is possible to relate these patterns to the differential cross section when the effects on the particle distribution of the harmonic potential and the projection onto the imaging plane are accounted for. As a result of the scattered particles expanding in an anisotropic harmonic potential, the projected halos seen in Fig. 2 have elliptical envelopes rather than the circle expected for a free-space Newton sphere as shown in Fig. 1. However, due to the cylindrical symmetry about the collision axis (which is perpendicular to the optical axis of our imaging system), full 3D tomographical information on the scattering can be extracted from the 2D absorption images via the inverse Abel transform [17,22]. Applying Abel inversion to the absorption images gives us the angular particle distribution in the trap at the time of image acquisition, to which the distribution at the time of collision (the free-space distribution) is related in a straightforward manner [23].

In Fig. 4(a) we show polar plots of the probability density $n_{sc}(\theta, T) \propto d\sigma/d\Omega$ for a scattered particle to be emitted at the polar angle $\theta$ as determined from the absorption images in Fig. 2. The angular distributions for different temperatures have been normalized with respect to each other such that $\int n_{sc}(\theta, T)d\Omega = 1$ for all $T$ and were determined from the Abel inverted images by counting the particles within angular bins at a unit sphere transformed to the quarter period ellipsoid via the relation in Ref. [23]. For comparison we present in Fig. 4(b) the temperature development of the normalized differential cross section as predicted by Eq. (1) using the partial-wave shifts from the previously described model. The scattering patterns of Figs. 4(a) and 4(b) show the same behavior and the minor discrepancies between the experimental and theoretical distributions may be attributed to

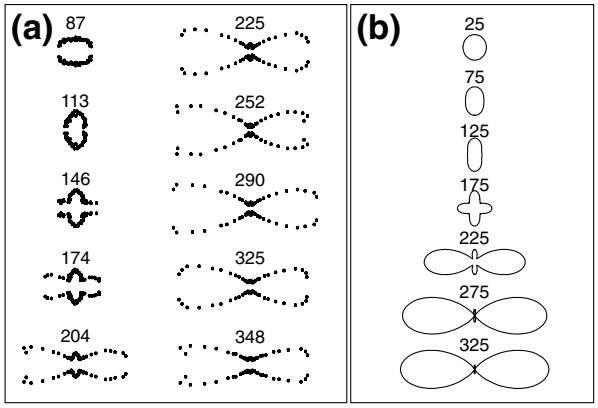


FIG. 4. Polar plots of the normalized angular scattering probability density for different collision energies in $\mu$K. (a) Experimental results from the absorption images of Fig. 2 after Abel inversion and a transformation from trap to free space. (b) Characteristic patterns as predicted by Eq. (1) using the partial-wave shifts from our theoretical model.

broadening effects from the finite sizes of the colliding clouds and a small departure from an ideal scattering geometry, both of which are not included in our analysis method [24]. For low temperatures the scattering is $s$-wave dominated and isotropic. However, at the onset of the $d$-wave scattering resonance the $s$ and $d$ partial-wave amplitudes interfere constructively in the radial direction and destructively in the axial direction. Above the $d$-wave resonance the scattering pattern is $d$-wave dominated, but nonvanishing $s$-wave scattering gives rise to destructive interference in the radial direction and constructive interference in the axial direction.

In conclusion, we have reported direct imaging of the scattered atoms in cold collisions of doubly spin-polarized $^{87}$Rb. The emission patterns and the measured number of scattered atoms as a function of collision energy are described well by a theoretical model. The present experiment demonstrates, in particular, the quantum mechanical nature of the scattering of atoms. The underlying quantum mechanics reveals itself strikingly through the appearance of one of its most prominent features—interference—and as only two states are involved in the scattering, the interpretation becomes particularly simple. On a more subtle level the extended version of Pauli's exclusion principle gives rise to the absence of odd partial waves since the scattering particles are identical bosons. Finally, we note the possibility of extending our method to other important low-lying resonances, atoms in different spin states, and to heteronuclear collisions.

This work was supported by the Marsden Fund of New Zealand, Contract No. 02UOO080. N. K. acknowledges additional support from the Danish National Science Research Council. We thank V. Dribinski for providing us with a software implementation of the Abel inversion method of Ref. [22].

*Electronic address: nk@physics.otago.ac.nz

[1] H. Faxén and J. Holtsmark, Z. Phys. **45**, 307 (1927).
[2] E. U. Condon and P. M. Morse, Rev. Mod. Phys. **3**, 43 (1931); P. M. Morse, *ibid.* **4**, 577 (1932).
[3] S. Chu, Rev. Mod. Phys. **70**, 685 (1998); C. N. Cohen-Tannoudji, *ibid.* **70**, 707 (1998); W. D. Phillips, *ibid.* **70**, 721 (1998).
[4] J. Weiner *et al.*, Rev. Mod. Phys. **71**, 1 (1999).
[5] M. H. Anderson *et al.*, Science **269**, 198 (1995); K. B. Davis *et al.*, Phys. Rev. Lett. **75**, 3969 (1995).
[6] B. DeMarco and D. S. Jin, Science **285**, 1703 (1999).
[7] J. M. Gerton *et al.*, Nature (London) **408**, 692 (2000).
[8] S. Inouye *et al.*, Nature (London) **392**, 151 (1998).
[9] E. A. Donley *et al.*, Nature (London) **417**, 529 (2002); C. A. Regal *et al.*, *ibid.* **424**, 47 (2003).
[10] S. Jochim *et al.*, Science **302**, 2101 (2003); M. Greiner, C. A. Regal, and D. S. Jin, Nature (London) **426**, 537 (2003); M.W. Zwierlein *et al.*, Phys. Rev. Lett. **92**, 120403 (2004).
[11] H. R. Thorsheim, Y. Wang, and J. Weiner, Phys. Rev. A **41**, 2873 (1990).
[12] R. Legere and K. Gibble, Phys. Rev. Lett. **81**, 5780 (1998).
[13] A. P. Chikkatur *et al.*, Phys. Rev. Lett. **85**, 483 (2000).
[14] H. M. J. M. Boesten *et al.*, Phys. Rev. A **55**, 636 (1997).
[15] S. Geltman, *Topics in Atomic Collision Theory* (Academic Press, New York, 1969).
[16] $l = \{1, 3, 5, \ldots\}$ terms are strictly forbidden and $l = \{4, 6, 8, \ldots\}$ terms have been calculated to be completely negligible for the energy interval of interest.
[17] R. N. Bracewell, *The Fourier Transform and Its Applications* (McGraw-Hill, Singapore, 2000), 3rd ed.
[18] T. Esslinger, I. Bloch, and T.W. Hänsch, Phys. Rev. A **58**, R2664 (1998).
[19] N. R. Thomas, A. C. Wilson, and C. J. Foot, Phys. Rev. A **65**, 063406 (2002).
[20] A. Marte *et al.*, Phys. Rev. Lett. **89**, 283202 (2002).
[21] During collisions the densities $n_i$ of the clouds labeled by $i = 1, 2$ are governed by the two coupled nonlinear partial differential equations $\partial_t n_i(x, y, z, t) = v_i \partial_z n_i \times (x, y, z, t) - |v|\sigma(T) n_1(x, y, z, t) n_2(x, y, z, t)$. Assuming the clouds to have initially Gaussian density distributions in all directions, this system was solved numerically to calculate the fraction of scattered particles and assess the scaling with the coupling parameter $\sigma(T)$. Because of the prolate cloud shapes we neglect multiple scattering events.
[22] V. Dribinski *et al.*, Rev. Sci. Instrum. **73**, 2634 (2002).
[23] A particle emitted in the polar angle $\theta_0$ at time $t = 0$ from the center of the trap follows a trajectory so that $\tan\theta(t) = \tan\theta_0 \omega_z \sin(\omega_r t)/\omega_r \sin(\omega_z t)$.
[24] As a consequence of the broadening, some scattered atoms reach their maximum radial excursion point before the time of image acquisition. This effectively transfers them to angular bins closer to the collision axis. The slight left-right pattern asymmetry observable for some collision energies is a combined result of the clouds having slightly different speeds in the laboratory frame, a small offset on the $z$ axis between collision and trap centers, and the size difference between colliding clouds [N. Kjærgaard, A. S. Mellish, and A. C. Wilson, New J. Phys. (to be published)].